Deep Resources Engineering 2 (2025) 100185

Contents lists available at ScienceDirect

Deep Resources Engineering

journal homepage: www.keaipublishing.com/en/journals/deepre/

Full Length Article

Numerical study on failure and instability of slender rock columns: Synergistic effects of lateral pressure, height-to-width ratio, and material strength

Shiguo Feng [a,b], Gen Li [a,b,*]

[a] State Key Laboratory of Coastal and Offshore Engineering, Dalian University of Technology, Dalian 116024, China
[b] Ocean Engineering Joint Research Center of DUT-UWA, Dalian University of Technology, Dalian 116024, China

ARTICLE INFO

Keywords:
Slender rock column
Material failure
Structural instability
H/W ratio
Material strength
Lateral pressure

ABSTRACT

Columnar jointed rock mass (CJRM) combines and mosaic of slender rock columns with different height-to-width (*H/W*) ratios. Revealing the correlation of the mechanical behavior of individual rock columns with internal factors (*H/W* ratio and material strength) and external factor (lateral pressure) is fundamental to understanding the deterioration of CJRM. We adopt a numerical scheme that combines a statistical meso-damage constitutive model with a finite element formulation based on finite deformation, which can simultaneously consider both material failure and structural instability of the rock columns. Compression tests of rock columns with different *H/W* ratios and material strengths under varying lateral pressures were conducted to analyze the macro-strength features and failure modes. The numerical results show that increasing the material strength can improve the macro-strength, while the effect of *H/W* ratio is the opposite. Both increases can promote the conversion of failure modes, and the evolution process is as follows: material failure-induced structural instability → synergy and competition between material failure and structural instability → structural instability-induced material failure. Notably, for the last failure mode, an increase in lateral pressure decreases the macro-strength of the rock column and heightens its instability risk. This finding provides new insights into the response of rocks with different *H/W* ratios under lateral pressure, extending beyond traditional material-based perspectives. According to the position of the failure mode demarcation line, the failure mode of the rock column can be regulated.

1. Introduction

Columnar jointed rock mass (CJRM) is a typical class of non-penetrating jointed rock mass formed during the cooling process of lava and distributed with relatively straight joint surfaces [1,2]. Many CJRMs have been exposed in projects such as the Baihetan Hydropower Station in southwest China, where structural surfaces are developed and spaced at small intervals with poor integrity (Fig. 1a) [3]. Due to the high initial in-situ stress value in the dam site area, the original tightly embedded columns of the CJRM relaxed and opened along the joint surfaces and micro-fractures under the excavation-induced stress unloading [4]. The rock columns' unique geometric effects and mechanical properties gradually emerge, threatening engineering safety. The study of its mechanical response and failure and instability mechanism is the prerequisite and foundation for deeply revealing the intricate deterioration mechanism of CJRM.

However, the current research objects of CJRM are mainly in-site engineering rock mass and rock column mosaic models (mosaic of different rock column combinations). The CJRM has a noticeable unloading relaxation effect and is highly susceptible to failure, such as rib spalling and buckling under high stress [5]. The distinctive structural surface induces conditions for the disintegration and spalling of the CJRM. The field investigations have revealed the formation of plate-columnar rock on the surface of the surrounding rock and the expansion of internal cracks utilizing borehole imaging technologies and displacement measurements. Spalling occurs gradually from the shallow surface to the interior [6]. The buckling and breaking of the rock column are the essential mechanisms that cause the progressive failure of the surrounding rock to the depth and even the occurrence of rock bursts. The field investigation results provide direct in-situ evidence of engineering catastrophe caused by the failure and instability of slender rock columns. Numerous scholars have carried out a large number of CJRM

* Correspondence to: Dalian University of Technology, No.2 Linggong Road, Ganjingzi District, Dalian City, Liaoning Province, China.
E-mail address: ligen8@dlut.edu.cn (G. Li).

https://doi.org/10.1016/j.deepre.2025.100185
Received 10 March 2025; Received in revised form 15 April 2025; Accepted 24 April 2025
Available online 25 April 2025

physical tests [7–11] and numerical experiments [12–16]. The models' size, shape, and material are often set artificially, with certain limitations. Moreover, these studies mainly focus on the model's mechanical response (e.g., anisotropy and size effect) and failure characteristics as a whole, which leads to the neglect and concealment of the contribution of a single rock column more often than not. In the uniaxial and triaxial tests of the CJRM physical model, apparent large-displacement and large-rotation failure phenomena such as bending, breaking, and rotating occurred (Fig. 1b, c), which provided objective and clear evidence for the failure and instability of the slender rock columns. Although the research on CJRM has been fruitful, it is still unclear how the slender rock columns, as the basic component unit of CJRM, deteriorate and affect the overall mechanical response.

Although there have been many studies of rocks with different H/W ratios, these are usually in the range of 4 and below, and the macro-strength tends to stabilize [17–20]. This range of H/W ratios is much lower than the findings of the field columns, and the corresponding regularity consensus no longer applies to slender columns. This is due to the fact that the more slender the structure, the more the bending effect gradually becomes apparent, and the geometric effect will not be negligible, especially for heterogeneous rock columns. For more slender structures, the apparent strength decreases further [21]. The geometric effects of structural bodies involve stability issues, and scholars have theoretically investigated the buckling instability behavior of rock mass [22–24]. Zhu et al. [25] considered the influence of the local bending effect in the anisotropic constitutive model based on Cosserat theory. Although the above theoretical studies have gained many new insights, they are all based on different assumptions. They cannot fully consider the rock's heterogeneous, discontinuous, and nonlinear nature, the material's failure, and the cracks' extension. It is conspicuous that the aforementioned experiments and theories focus respectively on material-level and structural-level studies, which are severed from each other. This leaves out the dynamic mechanisms of action that dominate and synergize with each other. Recently, the authors' research group developed a unified numerical scheme based on statistical meso-damage theory and finite deformation theory [26], which provides a powerful method for studying the failure and instability of rock mass. Preliminary explorations have been carried out for the effects of internal factors (e.g., H/W ratio and material strength) of rock columns [27,28]. However, the specific influence of lateral pressure as an external factor on the mechanical response of slender rock columns, as well as the failure and instability mechanisms of rock columns under the combined effect of internal and external factors, is a topic that requires urgent and in-depth study. This is the main objective of this study.

In this study, we adopt a unified numerical scheme based on the statistical meso-damage theory and finite deformation theory, which can simultaneously characterize the rock material's failure and the structural body's instability. Section 2 briefly reviews the unified numerical scheme. In Section 3, we establish the corresponding numerical models based on the dimensional and material parameters investigated at the CJRM site and the stress environment in which it is located. Numerical tests of slender rock columns with different H/W ratios and material strengths under different lateral pressures are carried out. The mechanical response and failure and instability mechanisms of the rock

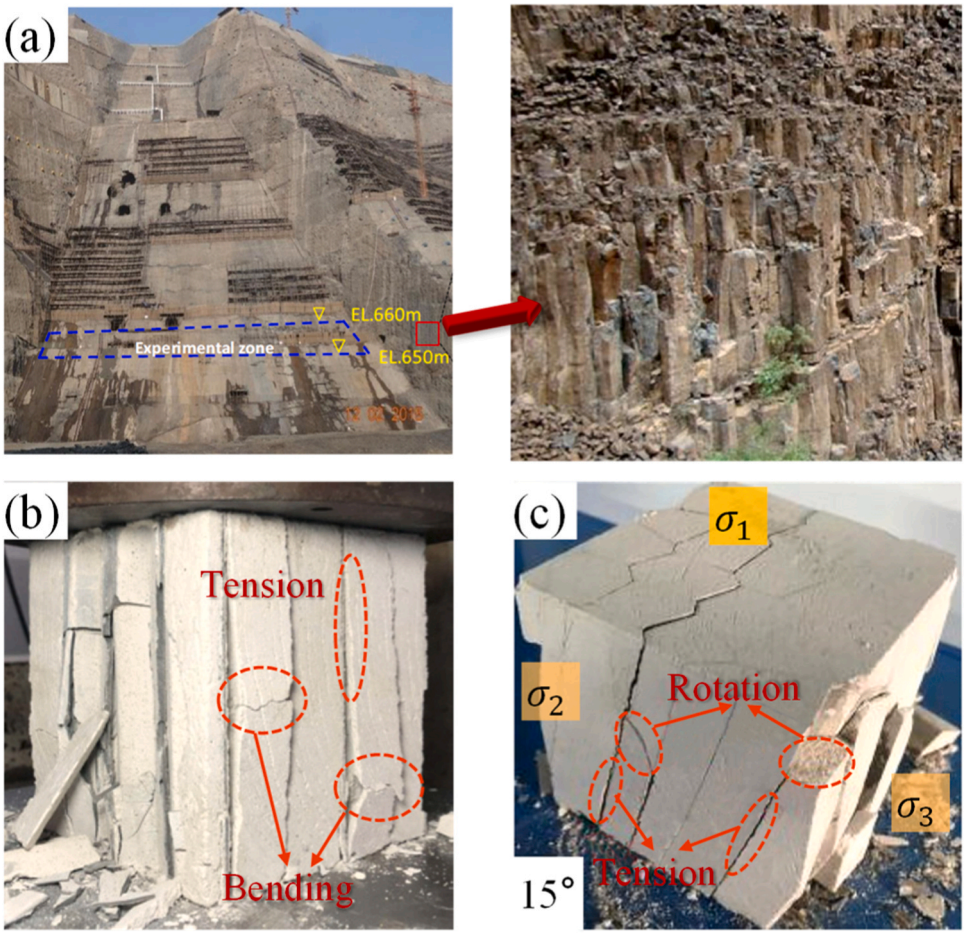

Fig. 1. (a) The CJRM stratum exposed at the dam foundation relaxed and disintegrated after excavation, and the rock columns buckled and broke [29]; (b) and (c) are the results of uniaxial and triaxial tests of artificial CJRM specimens, respectively [30,31]. Both of them experienced the disintegration of the CJRM, and the rock columns suffered from failure phenomena such as bending, breaking, and toppling.

columns under the combined effect of internal and external factors are investigated. The effect of lateral pressure on the macro-strength is discussed in detail. Section 4 draws some conclusions.

2. Methodology

2.1. Statistical Meso-damage Model

2.1.1. Statistical description of heterogeneity of rock material

There is a robust intrinsic correlation between the macro-properties and behavior of rock materials and the micro- and meso-scale organization and properties. The mechanical response of rock at the macro-scale can be understood in terms of the evolutionary mechanisms of microstructure at the meso-scale. Macroscopic experimental data can constrain the parameters of the mesoscopic model. In terms of material properties, the meso-heterogeneity of rock is the material root of the macro-nonlinearity [32]. The representative volume element (RVE) is homogeneous and isotropic at the meso-scale. The numerical model consists of a regular arrangement of elements with identical shapes and sizes, and one element represents one RVE [33]. Based on the statistical strength theory, the meso-scale inhomogeneity can be expressed by the parameters of the RVE obeying a specific statistical distribution function. Among them, the Weibull distribution is one of the ideal functions for describing the distribution of parameters of rock-like materials. The Weibull probability density function [34] is expressed as:

$$f(a) = \frac{m}{a_0}\left(\frac{a}{a_0}\right)^{m-1} \exp\left(-\left(\frac{a}{a_0}\right)^{m}\right) \tag{1}$$

where a is the mechanical parameter of the meso-element, such as elastic modulus and strength; a_0 is the average value of these parameters. m is known as the heterogeneity index, which represents the degree of non-uniformity of the material parameter. The larger the m value, the more homogeneous the material, and vice versa. $f(a)$ is the distribution density function of the material parameter, and the function for different heterogeneity indexes is shown in Fig. 2.

2.1.2. Double damage function

The stress state at a point in the rock can be expressed in the following three states:

$$F(\tilde{\boldsymbol{\sigma}}) < 0 \tag{2a}$$

$$F(\tilde{\boldsymbol{\sigma}}) = 0 \tag{2b}$$

$$F(\tilde{\boldsymbol{\sigma}}) > 0 \tag{2c}$$

where $\tilde{\boldsymbol{\sigma}} = [\sigma_1 \quad \sigma_2 \quad \sigma_3]^T$ is the principal stress vector. When a point is in an elastic state (including unloading), the stress satisfies Eq. (2a).

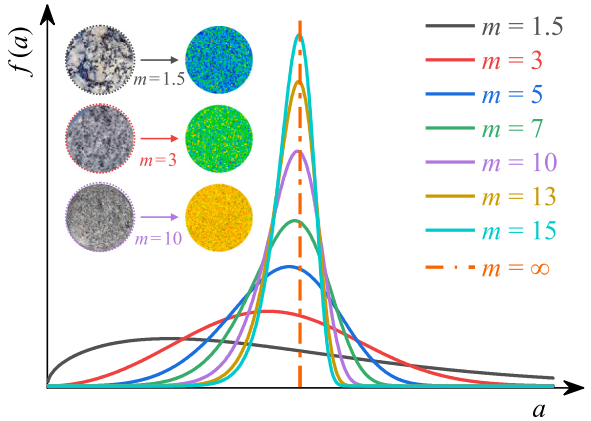

Fig. 2. Weibull distribution for different heterogeneity indexes.

When damage occurs at a point, the stress satisfies Eq. (2b). If a point subsequently continues to damage, the stress satisfies Eq. (2c). It is worth noting that this stress state (Eq. (2c)) does not exist in reality. The unrealistic stress needs to be pulled back to the damaged surface for subsequent damage evolution.

As a quasi-brittle material, the rock adopts an elastic-brittle damage description as Fig. 3. For the RVE in the elastic state, the loading and unloading responses satisfy the linear-elastic relationship. The damage of the RVE is categorized into tensile and shear damage. When the RVE stress reaches the initial damage surface $F_0^{\pm} = 0$, a brittle drop in stress occurs. The " $\pm$ " notation designates the elemental stress states: the '+' symbol denotes compressive stress states, while the '-' symbol represents tensile stress states. Since the rock usually still has a specific residual bearing capacity after failure, the residual strength surface is considered as the subsequent damage surface $F_1^{\pm} = 0$ in this study. The damage evolution of RVE will be confined to the damaged surface $F_1^{\pm}$ until the final failure occurs. The failure judgment of RVE is based on the Mohr-Coulomb criterion with tensile truncation. The tensile and shear damage functions are denoted as:

$$F_0^{-}(\tilde{\boldsymbol{\sigma}}) = \sigma_3 + f_t = 0 \tag{3a}$$

$$F_0^{+}(\tilde{\boldsymbol{\sigma}}) = \sigma_1 - \sigma_3\frac{1+\sin\theta}{1-\sin\theta} - f_c = 0 \tag{3b}$$

where f_t and f_c are the uniaxial tensile and compressive strength, respectively; σ_1 and σ_3 are the maximum and minimum principal stresses, respectively; and θ is the friction angle.

The subsequent tensile damage surface F_1^{-} and shear damage surface F_1^{+} are formulated as follows:

$$F_1^{-}(\tilde{\boldsymbol{\sigma}}) = \kappa_t f_t = f_{rt} \tag{4a}$$

$$F_1^{+}(\tilde{\boldsymbol{\sigma}}) = \kappa_c f_c = f_{rc} \tag{4b}$$

where κ_t and κ_c denote the residual strength coefficients under tensile and compressive states respectively, while f_{rt} and f_{rc} correspond to the residual tensile strength and residual compressive strength. Tensile damage is the first damage criterion. If no tensile damage occurs, shear damage judgment is performed [33]. The RVE in this study can only have one damage (failure) state at the same time.

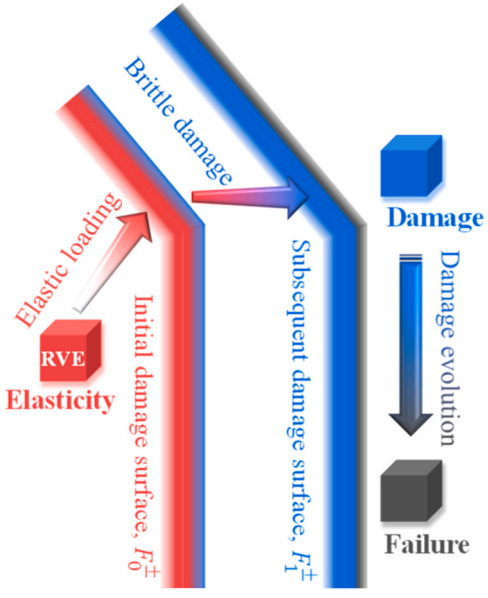

Fig. 3. Damage evolution process and different states of RVE.

2.1.3. Damage evolution law

The macroscopic deterioration of rock is essentially the weakening of the stiffness and the reduction of the strength of the meso-scale elements. According to the isotropic damage theory [35], the damage variables can be expressed in material parameters. This study uses the Young's modulus to define the damage variable ϖ.

$$\varpi = 1 - \frac{Y^{\pm}}{Y_0} \tag{5}$$

where $Y^{\pm}$ and Y_0 are Young's modulus for the damaged and undamaged states, respectively. Based on the strain equivalence principle [36], the stress-strain relationship for elastic brittleness is expressed as:

$$\varepsilon = \sigma(1-\varpi)Y_0 \tag{6}$$

The stress-strain relationship of RVE under uniaxial compression or tension is shown in Fig. 4. The damage evolution equation in the tensile state is:

$$d = \begin{cases} 0 & \varepsilon > \varepsilon_{t0} \\ 1 - \dfrac{f_{rt}}{\varepsilon Y_0} & \varepsilon_{tl} \le \varepsilon \le \varepsilon_{t0} \\ 1 & \varepsilon < \varepsilon_{tl} \end{cases} \tag{7}$$

where f_{rt} is the residual tensile strength; ε_{t0} and ε_{tl} are the strain thresholds at the elastic limit and tensile limit, respectively. For complex stress states, ε in Eq. (7) can be replaced by the equivalent maximum tensile strain. If the stress state of RVE reaches the shear damage criterion, the damage evolution equation is:

$$d = \begin{cases} 0 & \varepsilon < \varepsilon_{c0} \\ 1 - \dfrac{f_{rc}}{\varepsilon Y_0} & \varepsilon_{c0} \le \varepsilon \le \varepsilon_{cl} \end{cases} \tag{8}$$

where f_{rc} is the residual compressive strength; ε_{c0} and ε_{cl} are the strain thresholds at the elastic limit and compressive limit, respectively. ε is the strain in uniaxial compression or the maximum compressive principal strain in the multiaxial stress state.

Element failure occurs when the strain attains the limit strain. Failed elements are assigned minimal stiffness, and their color is adjusted to the background color. The smearing treatment of failed elements inherently characterizes complex fracture behaviors such as crack initiation, propagation, and coalescence. If failed elements undergo high compression, their stiffness recovers to the initial value, and no further damage analysis is performed. Stiffness-recovered elements regain stress-transfer capacity with neighboring elements. When the strain of highly compressed elements is less than the limit strain, they are reprocessed as failed elements. Detailed damage evolution mechanics are documented in [33].

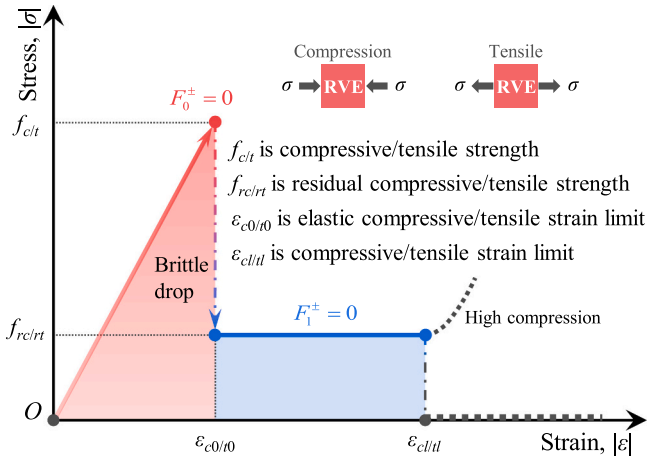

Fig. 4. Stress-strain relationship of RVE in compression and tension in a one-dimensional state.

2.2. Finite element approximation of finite deformation

For traditional rock deformation analysis, using small deformation theory usually gives satisfactory results with acceptable errors. However, the finite deformation theory is needed when the rotation and deformation are large. The deformation of slender rock columns, such as bending and breaking, belongs to the problem of large displacement and small strain. The stress-strain relationship of elastic-brittle rock can still use Hooke's law. However, the definitions of strain and stress need to satisfy the energy conjugate principle [37]. This study adopts the Total Lagrange method, taking the configuration at the initial moment as the reference configuration. According to the principle of virtual displacement, the equilibrium equation is established as follows:

$$\{du\}^T\{R\} = \int_{\Omega}\{d\varepsilon\}^T\{\sigma\}dV - \{du\}^T\{Q\} = 0 \tag{9}$$

where $\{du\}$ and $\{d\varepsilon\}$ are the virtual displacement and virtual strain, respectively. $\{R\}$ is the sum of the internal and external force vectors at the node. $\{Q\}$ is the load array. The strain and displacement relationship in incremental form is expressed as:

$$\{d\varepsilon\} = [B]\{du\} = ([B_0] + [B_L])\{du\} \tag{10}$$

where $[B_0]$ is the strain matrix for linear strain analysis independent of node displacement; $[B_L]$ is the strain matrix caused by nonlinear deformation related to node displacement, which is generally a linear displacement function.

The stress-strain relationship is described by linear elasticity.

$$\{\sigma\} = [D]\{\varepsilon\} = (1-\varpi)[D_0]\{\varepsilon\} \tag{11}$$

where $[D]$ is the elastic matrix incorporating the evolution of material damage. Considering the arbitrariness of the virtual displacement, Eq. (9) is further simplified and differentiated to obtain:

$$\{dR\} = \int_{\Omega}[dB]^T\{\sigma\}dV + \int_{\Omega}[B]^T\{d\sigma\}dV = 0 \tag{12}$$

Bringing the displacement-strain matrix $[B]$ into Eq. (12) and expanding it yields

$$\{dR\} = [K]\{du\} = ([K_0] + [K_\sigma] + [K_L])\{du\} = 0 \tag{13}$$

where the tangent stiffness matrix $[K]$ can be decomposed as:

$$[K_0] = \int_{\Omega}[B_0]^T[D][B_0]dV \tag{14}$$

$$[K_\sigma]\{du\} = \int_{\Omega}[dB_L]^T\{\sigma\}dV \tag{15}$$

$$[K_L] = \int_{\Omega}[B_0]^T[D][B_L]dV + \int_{\Omega}[B_L]^T[D][B_L]dV + \int_{\Omega}[B_L]^T[D][B_0]dV \tag{16}$$

where $[K_0]$ is the material stiffness matrix, independent of the node displacement. It describes the contribution of material properties to the system stiffness, dominating the elastic response under small deformation; $[K_\sigma]$ is the geometric stiffness matrix, which describes the contribution of the geometric state to the system stiffness, reflecting the effect of the initial stress on the stiffness. $[K_L]$ is the initial displacement matrix or large displacement matrix related to the load changing with deformation. It is currently assumed that the derivative of the load term is zero, so $[K_L]$ disappears. The equations of this study are solved using the Newton-Raphson iterative method.

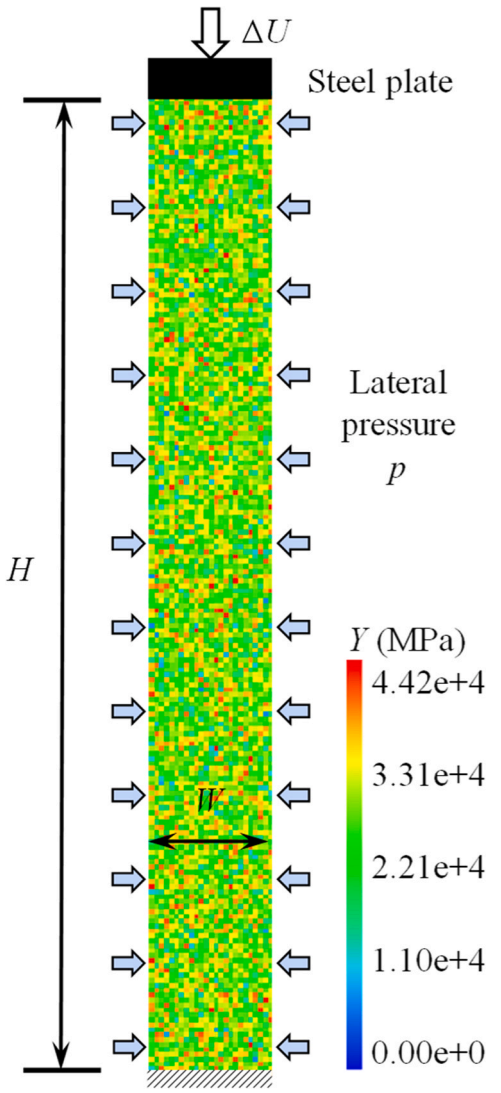

Fig. 5. Geometric model and boundary conditions of rock column under lateral pressure.

3. Numerical simulation

3.1. Model Setup

The geological survey of Baihetan Hydropower Station classified the CJRM into three categories based on the development of joints and the size of rock columns [38]. Among them, the Category-I rock mass has a greater density of columnar joint development and is widely distributed in the middle and lower parts of the dam foundation. The columns have a length of 2–3 m and a diameter of 13–25 cm, which have apparent shape effects. According to the size and material characteristics of the Category-I CJRM, as well as the in-situ stress environment, the numerical model shown in Fig. 5 was developed to investigate the effects of *H/W* ratio, lateral pressure, and material strength on the macro-strength and failure and instability characteristics of the rock columns at the engineering scale. The *H/W* ratios of the rock column are proposed to be 8, 10, and 12. The model's width is kept at 25 cm, and the height is variable. The size of each element of the numerical model is 1 cm × 1 cm, considering the computational efficiency and the block size of the rock mass in the field. The lateral pressures of the model are selected to be 0 MPa, 5 MPa, 10 MPa, and 15 MPa, in which the model at 0 MPa is an ordinary uniaxial compression model of the rock column without lateral pressure. The material strength refers to the meso-uniaxial compressive strength of the material in the numerical model, which has the same meaning in this paper. The macro-strength refers to the critical stress at which rock columns experience failure and instability, manifested as the peak stress on the stress-strain curve. This study sets up the numerical scheme combining the three factors of *H/W* ratio, lateral pressure, and material strength. The specific parameters of the model are listed in Table 1. The model is fixed at the bottom, the initial lateral pressure is applied on both sides, and the displacement load ΔU is applied at the top by a steel plate until the model fails.

3.2. Effects of lateral pressure, H/W ratio, and material strength on mechanical properties of rock columns

Fig. 6 shows the stress-strain curves of rock columns with different *H/W* ratios (*H/W* = 8, 10, and 12) and material strengths (f_{mc} = 100 MPa, 300 MPa, and 500 MPa) for various lateral pressures (p = 0, 5, 10, and 15 MPa.).

From Fig. 6, it can be seen that the pre-peak stress-strain curves of rock columns with a specific *H/W* ratio overlap at the same lateral pressure, and the peak stress varies due to the material strength. As the *H/W* ratio increases (e.g., *H/W* = 12, f_{mc} = 500 MPa,) the nonlinear characteristics of the stress-strain curves of the rock columns become more apparent. In particular, the curves gradually bend and flatten near the peak stress and drop rapidly after a short period of deformation, which implies that the rock columns have undergone sudden and catastrophic instability failure [39]. Moreover, it is also evident that the stress-strain curve of the rock column with lateral pressure is above the curve without lateral pressure. This is because the lateral pressure is applied as an initial condition, and axial compressive strain occurs only when the vertical displacement load is applied to a specific value, owing to the Poisson effect in the initial loading stage.

In order to fully reveal the macro-strength characteristics of the rock columns under the influence of the three factors, two-dimensional macro-strength point-line diagrams were plotted as well as strength space surfaces were established in the space consisting of *H/W* ratio-material strength-lateral pressure and macro-strength, and plane projections were performed (Figs. 7–9). There is an apparent dividing line on the strength space surface (e.g., the black dotted line in Fig. 7b), and the macro-strength change trends are different on both sides, which we call the macro-strength change trend demarcation line.

Fig. 7 shows that the macro-strength of the rock column decreases with increasing *H/W* ratios, which is consistent with the view of [27].

Table 1
Numerical model parameters of the rock column under lateral pressure.

Parameters	Values
H/W ratio	8, 10, and 12
Numerical model size *H* (cm)× *W* (cm)	200 × 25, 250 × 25, and 300 × 25
Meso-uniaxial compressive strength, f_{mc} (MPa)	100, 300, and 500
Meso-Young's modulus, Y_0 (MPa)	30000
Ratio of meso-uniaxial compressive and tensile strength	10
Lateral pressure, p (MPa)	0, 5,10, and 15
Heterogeneity index, m	5

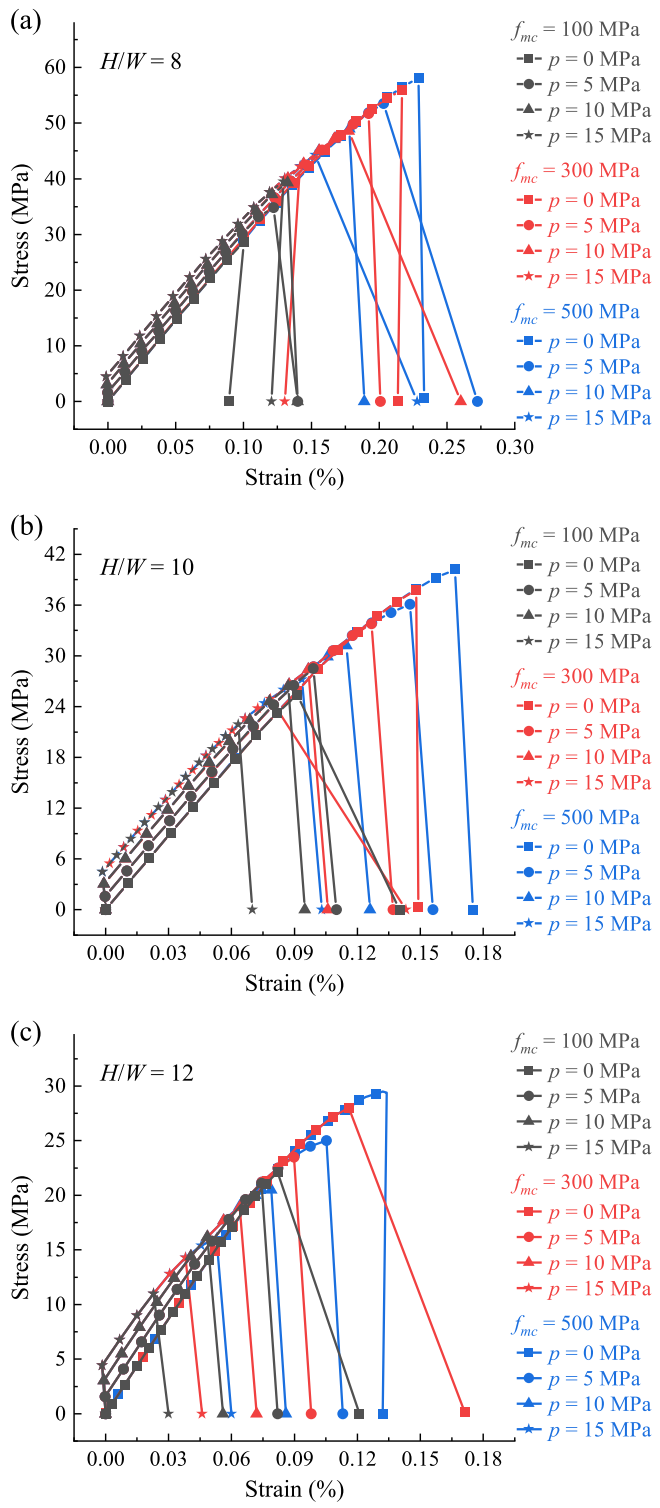

Fig. 6. Stress-strain curves of rock columns with H/W ratios of (a) 8, (b) 10, and (c) 12 at different lateral pressures and different material strengths.

The macro-strength trend demarcation divides the macro-strength spatial surface into two regions, A and B. In Fig. 7b, the spatial location relationship in region A indicates that the effect of the H/W ratio on the decrease of the macro-strength is weaker when the material strength and lateral pressure are lower. At this time, increasing the material strength and lateral pressure can increase the macro-strength and enhance the effect of the H/W ratio on the macro-strength. Fig. 7a and b reflect that the H/W ratio vs. macro-strength relationship curves (or spatial surface B region) are approximately parallel for high material strength and high lateral pressure, which indicates that the H/W ratio is the dominant factor influencing the macro-strength.

Fig. 7c-e show that the effects of lateral pressure and material strength on macro-strength are most pronounced for rock columns with $H/W = 8$. The strength contours are densest in region A, with the most extensive range of macro-strength variations (28.57 MPa-55.92 MPa). The strength value is lowest at the origin of the coordinates ($p = 0$ MPa, $f_{mc} = 100$ MPa) (Fig. 7c). As the H/W ratio increases, the shape effect of the rock column increases, and the risk of instability increases. The contours in region B gradually flatten out, and the contours in region A become sparse, which implies that the influence of material strength on the macro-strength is weakened, and the increase of lateral pressure promotes the failure and instability of rock columns. The final minimum value of macro-strength appears in region B ($p = 15$ MPa, $f_{mc} = 100$ MPa).

It is apparent from Fig. 8a that the macro-strength of the rock column increases with the increase of lateral pressure at low H/W ratio ($H/W = 8$) and low material strength ($f_{mc} = 100$ MPa), which is consistent with the conventional knowledge of the compressive strength law of rock, that is, lateral pressure can enhance the bearing capacity of rocks [40]. However, when the H/W ratio and material strength reach a certain threshold, the macro-strength of the rock column decreases with the increase of lateral pressure.

Fig. 8b shows that the macro-strength spatial surfaces of rock columns at different lateral pressures intersect. The macro-strength of rock columns at low H/W ratio ($H/W = 8$) and low material strength ($f_{mc} = 100$ MPa) at $p = 0$ MPa and 5 MPa is lower than that at $p = 15$ MPa. As the lateral pressure increases (e.g., $p = 10$ MPa), the macro-strength becomes higher than that of $p = 15$ MPa. The macro-strength at a high H/W ratio and high material strength gradually decreases with increasing lateral pressure, and the strength spatial surfaces are approximately parallel to each other. It indicates that the effect of lateral pressure on the macro-strength of the rock column has a stage-by-stage nature. In contrast to the monotonicity of H/W ratios on the weakening of the macro-strength, the lateral pressure will dominate after increasing to a certain degree, and then reduce the macro-strength. In Fig. 8c-f, with the increase of lateral pressure, region A tends to decrease, the contour lines in region A gradually become sparse, and the angle between the contour lines on both sides of AB gradually becomes larger until it is smooth. It indicates that with the increase of lateral pressure, the macro-strength of the rock column becomes less sensitive to the change of the material strength, which is mainly affected by the H/W ratio. The macro-strength of the rock column with $H/W = 12$ and $f_{mc} = 100$ MPa is minimized at different lateral pressures. This is because an increase in the H/W ratio increases the instability risk of the columns, and an increase in material strength can improve the macro-strength to a certain extent [27]. The synergistic effect of the two puts the columns at higher instability risk under the above conditions.

Fig. 9 shows that the macro-strength of the rock column increases with increasing material strength. Fig. 9a clearly shows that the increase in material strength at low H/W ratios (e.g., $H/W = 8$) and low lateral pressures (e.g., $p = 0$, 5, and 10 MPa) significantly increases the macro-strength of the columns. For higher H/W ratios and lateral pressures, the effect of material strength on the macro-strength of the columns diminishes, and the line graphs are approximately straight and parallel. This law is specifically manifested in the strength spatial surface (Fig. 9b), which shows that the strength spatial surface has a good spatial hierarchical relationship under different material strengths, with the spatial surface in region A falling obviously and the spatial surface in region B being approximately parallel. It can be seen that the influence of material strength on macro-strength also has a dominant role. In Fig. 9c-e, the minimum value of the macro-strength all appeared at $H/W = 12$ and $p = 15$ MPa, but the location of the maximum value is different. When the material strength is low (Fig. 9c), the effects of lateral pressure and H/W ratio on macro-strength are poorly

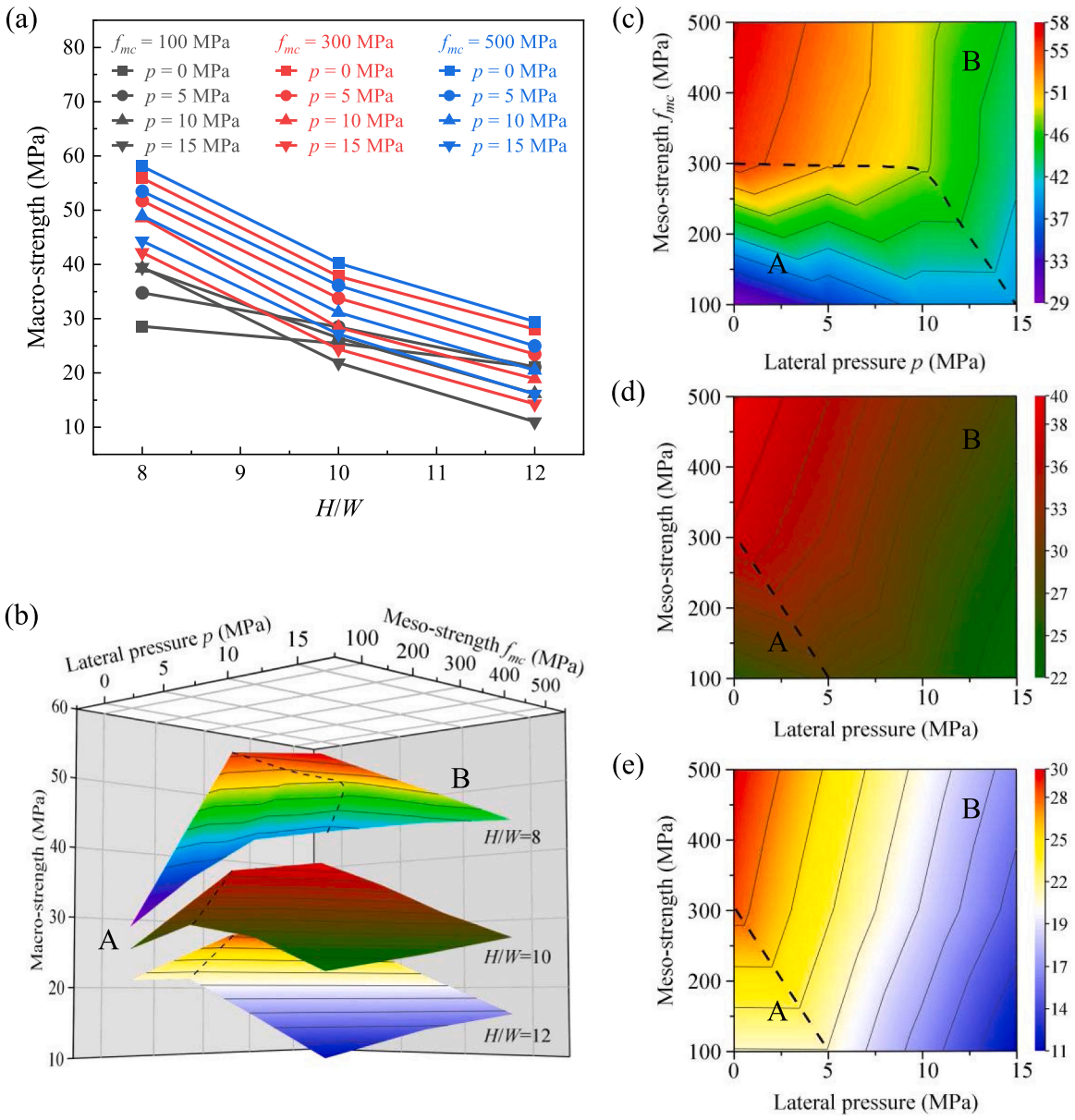

Fig. 7. Macro-strength of rock columns with different H/W ratios at different lateral pressures and different material strengths in (a) line graphs, (b) spatial surfaces and planar projections of (c) $H/W = 8$, (d) $H/W = 10$, and (e) $H/W = 12$. The colors in the spatial surfaces and projections represent the magnitude of the macro-strengths, and the solid black lines are the macro-strength contours.

coordinated. The macro-strength maximum occurs at $H/W = 8$, $p = 15$ MPa. When the material strength is high (Fig. 9d-e), the effects of lateral pressure and H/W ratio on the macro-strength are well-coordinated, and the macro-strength gradually decreases with the simultaneous increase of both. The maximum macro-strength value occurs at the origin (i.e., $H/W = 8$, $p = 0$ MPa).

Combined with the analysis of Figs. 7–9, it can be seen that the effects of the three factors on the macro-strength are differentiated. Compared with the internal factors (H/W ratio and material strength), the influence of external factor, lateral pressure, has obvious stages. The most unfavorable combination of the three factors can be determined through the position of the minimum macro-strength, specifically: $H/W = 12$, $f_{mc} = 100$ MPa, and p = 15 MPa. The analysis above reveals the variation trends of macro-strength under different factor combinations. The analysis of variance (ANOVA) was employed to evaluate the significance of the effect of each factor on macro-strength, with results presented in Table 2. The analysis incorporated second-order effects to account for factor interactions. A coefficient of determination (R^2 = 0.980) indicates strong explanatory power of the analytical model for strength variability. The larger F-values and smaller P-values demonstrate that the effect of factors is statistically significant.

Within the experimental scope of this study, the ANOVA results demonstrate that single-factor effects exhibit significantly greater influence on macro-strength compared to dual-factor interactions. Among individual factors, the significance hierarchy follows: H/W ratio > material strength > lateral pressure. For dual-factor combinations, the H/W ratio and material strength show the strongest significance, followed by lateral pressure and material strength. The lateral pressure and H/W ratio are insignificant on macro-strength. The disparity in statistical significance indicates that intrinsic factors (H/W ratio and material strength) dominate over extrinsic factors (lateral pressure) in governing macro-strength. Notably, the H/W ratio as the core geometric characteristic parameter of rock columns exhibits predominant control over macro-strength. Therefore, the H/W ratio should be prioritized as the primary control parameter in rock column stability analysis and engineering design.

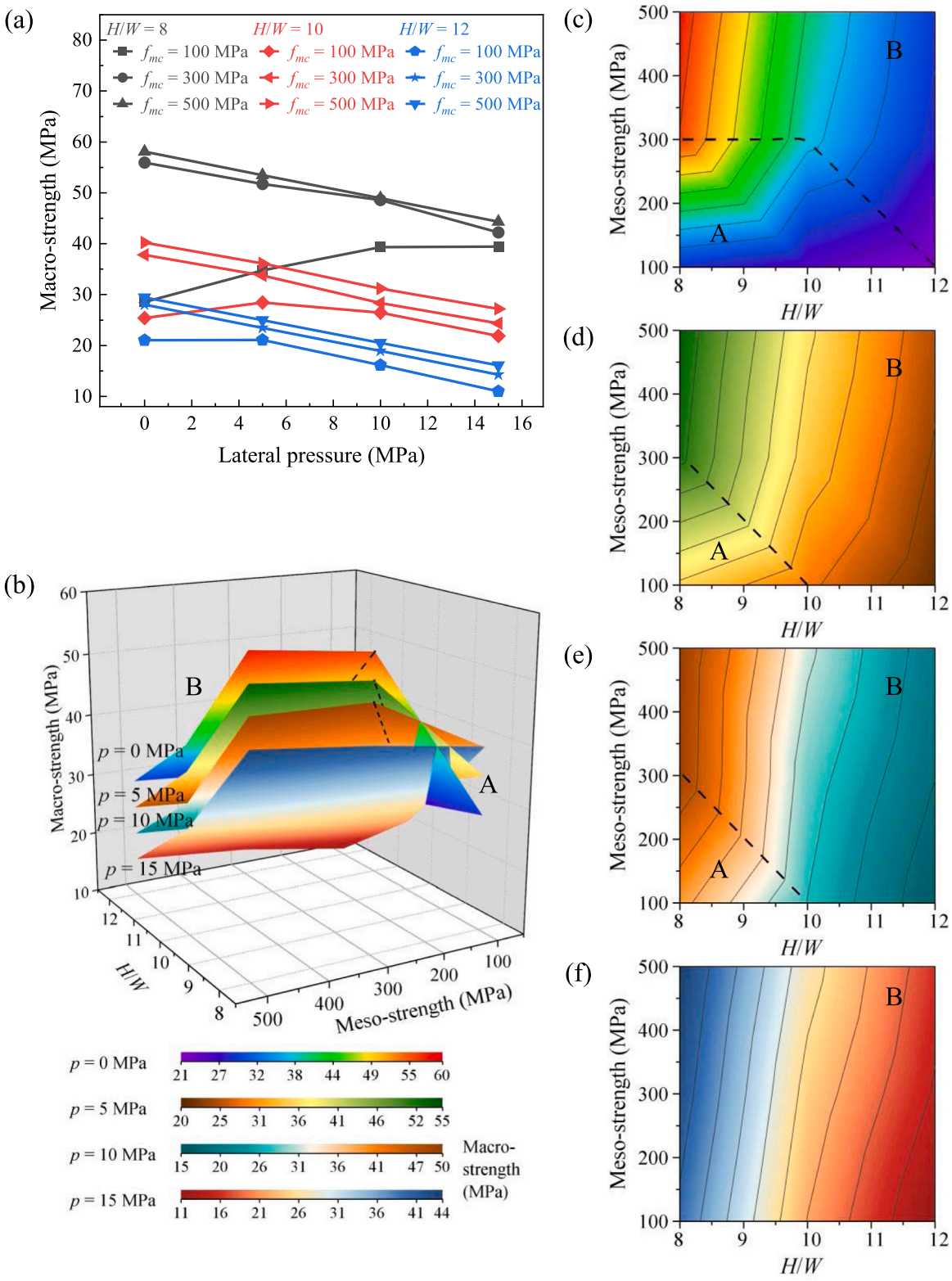

Fig. 8. Macro-strength of rock columns with different lateral pressures at different H/W ratios and different material strengths in (a) line graphs, (b) spatial surfaces and planar projections of (c) $p = 0$ MPa, (d) $p = 5$ MPa, (e) $p = 10$ MPa, and (f) $p = 15$ MPa.

3.3. Effects of lateral pressure, H/W ratio, and material strength on the failure mode of rock columns

Li et al. [27] preliminarily investigated the failure modes of rock with different H/W ratios. This study summarizes the typical features of the failure modes of intact rock columns under different H/W ratios. Typical features of the material failure-induced structural instability: The rock column undergoes macroscopic shear failure or vertical splitting failure, with macroscopic inclined fracture surfaces or severe localized failure; the failure location has a certain randomness, which is affected by factors such as loading conditions, material homogeneity; and the failure process has a gradual nature. Typical features of the

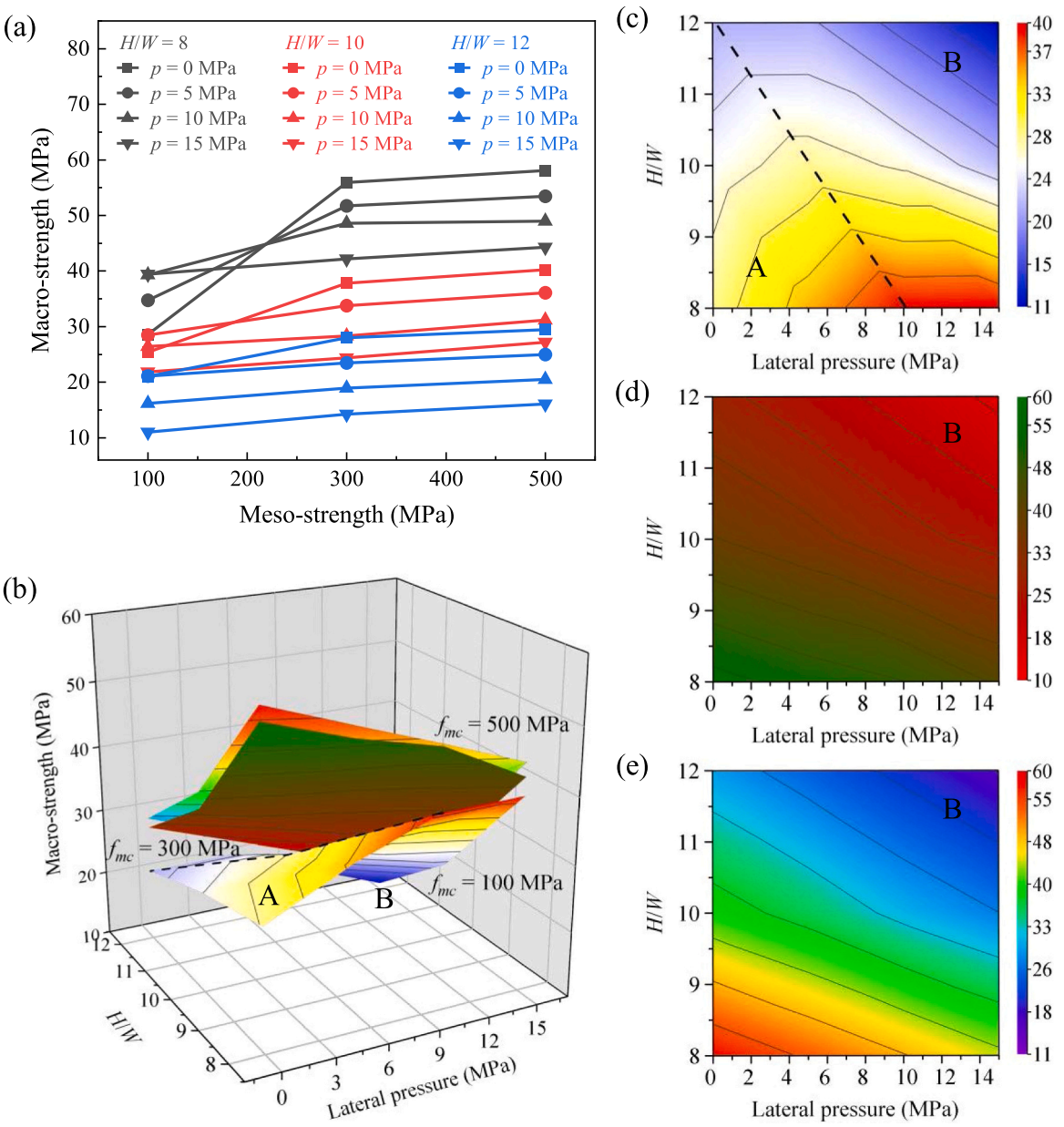

Fig. 9. Macro-strength of rock columns with different material strengths at different H/W ratios and different lateral pressures in (a) line graphs, (b) spatial surfaces and planar projections of (c) f_{mc} = 100 MPa, (d) f_{mc} = 300, and (e) f_{mc} = 500 MPa MPa.

Table 2
Results of three-factor analysis of variance.

Factors	Square sum	Degree of freedom	Mean square	*F* value	*P* value
Lateral pressure	413.098	3	137.699	15.459	0.000 * *
H/W ratio	3867.364	2	1933.682	217.092	0.000 * *
Material strength	580.923	2	290.462	32.610	0.000 * *
Lateral pressure and *H/W* ratio	56.236	6	9.373	1.052	0.440
Lateral pressure and material strength	193.001	6	32.167	3.611	0.028 *
H/W ratio and material strength	173.238	4	43.309	4.862	0.015 *

Note: $R^2 = 0.980$, * $P < 0.05$, * * $P < 0.01$

structural instability-induced material failure: The rock column undergoes large displacement and rotation angle, and the geometric shape after deformation obviously deviates from the original contour line. The failure of the rock column has a certain abruptness. The material tensile failure occurs in its tensile side's middle and lower position, and the cracks develop and expand laterally [41]. This kind of failure is catastrophic for the project. The synergy and competition between material failure and structural instability are related to the first two modes and are characterized by a combination of both. Material failure and significant rotation (bending) occur and compete and synergize with each other. The rock column finally fails in a synergistic failure and instability.

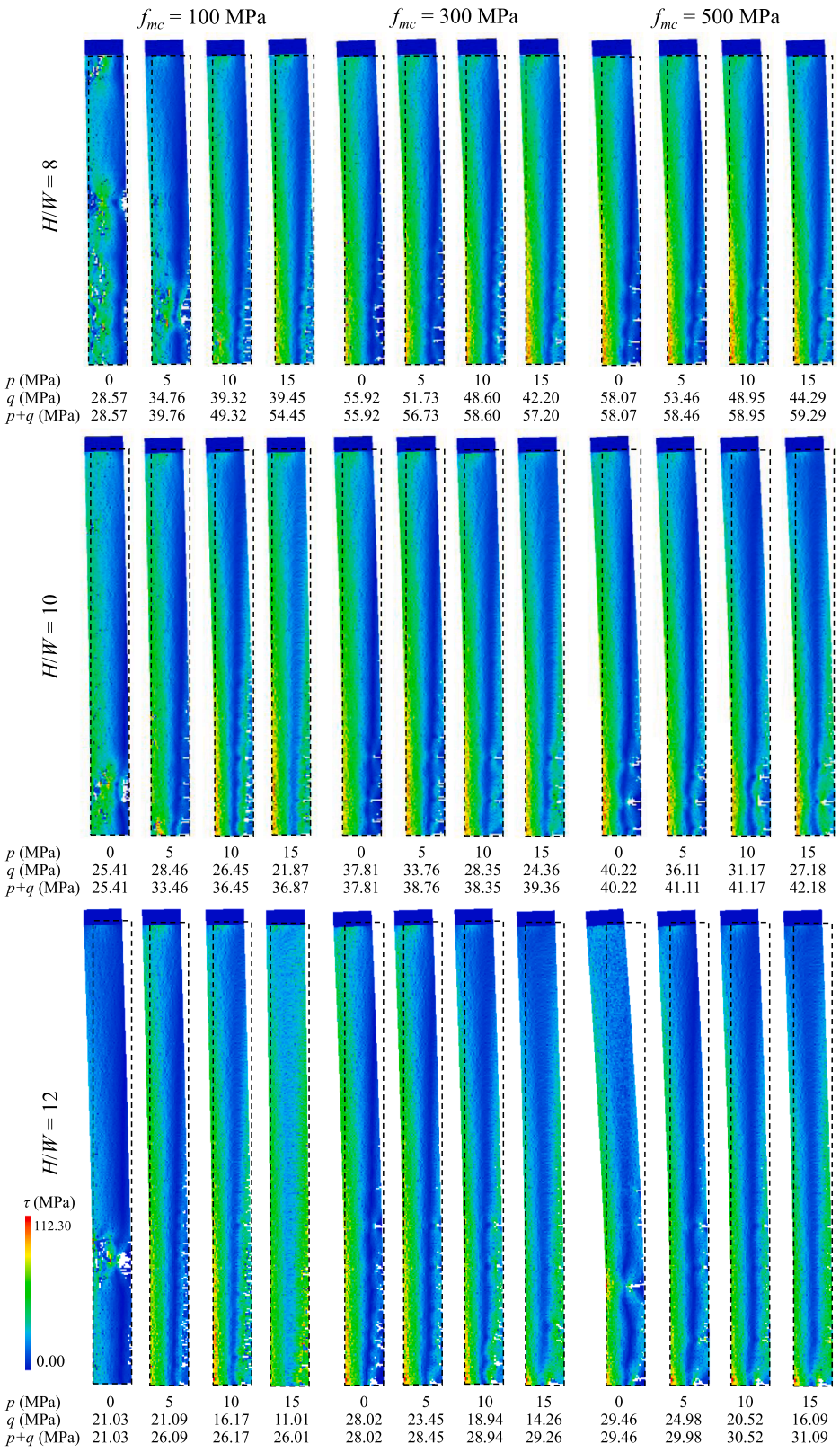

Fig. 10. The shear stress nephograms at the failure of rock columns under different H/W ratios, material strengths, and lateral pressures (p denotes the lateral pressure, q denotes the macro-strength, and $p + q$ is the sum of the lateral pressure and the macro-strength).

Fig. 10 shows the failure characteristics of the rock columns under different combinations of lateral pressure, H/W ratio, and material strength. The failure modes of the rock columns can be judged and classified according to the characteristics of the different failure modes summarized above.

Case 1- $H/W = 8$, $f_{mc} = 100$ MPa: The failure mode of the rock columns at $p = 0$ MPa is a material failure-induced structural instability. The specific failure process is shown in Fig. 11a. Initially, the rock

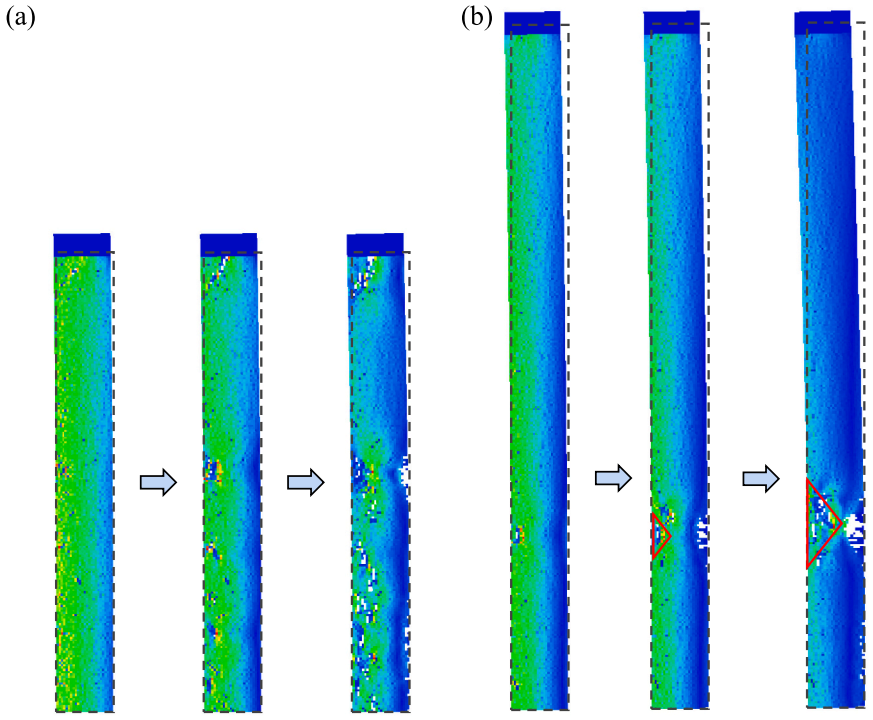

Fig. 11. The failure process of the rock column for $p = 0$, $f_{mc} = 100$ MPa at (a) $H/W = 8$ and (b) $H/W = 12$. The red solid line frame in (b) illustrates the outline of the "V" shaped failure zone.

column randomly distributes many stress concentration points. As the load continues to be applied, microcracks appear and develop, and multiple local failure zones appear along the height of the column, forming a macroscopic shear failure zone and a local splitting failure zone. The rock column finally fails and is unstable. With the increase of lateral pressure (e.g., $p = 5$ and 10 MPa), the material failure area on the compression side of the column gradually decreases, and the transverse cracks on the tensile side due to the more considerable bending deformation of the column increase. It implies that the failure process of the column is accompanied by mutual competition and synergy between the material failure and structural instability. At this time, the failure mode of the rock column is the synergy between material failure and structural instability. When $p = 15$ MPa, the failure characteristics of the column are the initiation and development of transverse cracks caused by the bending deformation of the structure, and the failure mode is a structural instability-induced material failure.

Case 2- $H/W = 10$, $f_{mc} = 100$ MPa: When $p = 0$ MPa, the failure mode of the rock column is a material failure-induced structural instability. Compared with case 1, the column also showed multiple stress concentration points. However, due to the enhanced structural effect (i.e., increase in H/W ratio), the rock column mainly experienced material failure in the bottom stress concentration area, which led to the final instability and failure. With the increase of lateral pressure, the material failure on the compression side is suppressed, and more transverse cracks are generated on the tension side due to the bending deformation. The failure mode has evolved from the synergy between material failure and structural instability to structural instability-induced material failure.

Case 3- $H/W = 12$, $f_{mc} = 100$ MPa: When $p = 0$ MPa, the failure mode of the rock column is the synergy between material failure and structural instability. The specific failure process is shown in Fig. 11b. The bending deformation of the rock column causes localized material failure on the compression side, which will cause the bending deformation of the rock column to increase and tensile cracks to emerge on the tensile side of the rock column. As the load continues to increase, the local "V"-shaped fracture zone on the compression side develops and expands, and the crack on the tension side develops and extends. The interaction of the two failure patterns leads to the final failure and instability of the rock column. With the increase of lateral pressure, the failure characteristics of the rock column are mainly the lateral tensile crack extension generated by the structural instability, and the failure mode is the structural instability-induced material failure.

Case 4- $H/W = 8$, $f_{mc} = 300$ MPa: The failure mode of the rock columns with $p = 0$ MPa referenced to Cases 1–3 is the synergy of material failure and structural instability. With the increase of H/W ratio, material strength, and lateral pressure, the failure modes of the rock columns in all other cases are the structural instability-induced material failure. The increase in the H/W ratio and material strength reduces the transition threshold between the failure modes, the bending deformation increases, and the instability risk increases. The increase in material strength makes the fracture area of the column concentrate from dispersezd, and the failure depth increases. The increase in lateral pressure also reduces the transition threshold between failure modes. However, it will limit the bending deformation of the rock column, leading to incomplete crack development and increasing the risk of sudden instability, which is similar to the view of Qiu et al. [42]. In addition, the greater the H/W ratio (i.e., the more slender the rock column), the more apparent the effect of lateral pressure on the stress distribution. The increase in lateral pressure concentrates the low shear stress zone near the central axis while developing from a unilateral distribution to a uniform distribution in the upper part of the rock column.

It can also be found from Fig. 10 that the evolution of the failure mode of the rock column corresponds well with the macro-strength trend. Therefore, the black dotted line in the spatial surface and planar projection of the macro-strength in Figs. 7–9 is not only the demarcation line of the macro-strength trend but also the demarcation line of the evolution of the failure mode. Near the demarcation line, the failure mode is the competition and synergy between material failure and structural instability. In region A, the failure mode is a material failure-induced structural instability; In region B, the failure mode is a structural instability-induced material failure. With increased lateral pressure, H/W ratio, and material strength, the strength contour is

gradually smoothed, and the failure mode transition threshold is lowered. The A region gradually transitions to the B region; that is, the evolution process of the failure mode is the material failure-induced structural instability → synergy and competition between material failure and structural instability → structural instability-induced material failure.

The above analysis shows that the conversion of failure mode is a dynamic evolution process of competition and synergy between material failure and structural instability rather than a sudden change process. Therefore, the failure mode of rock columns can be regulated by changing the lateral pressure, H/W ratio, and material strength along the macro-strength contour according to the location of the failure mode demarcation line. For rock column structures, we can always reduce the impact of structural instability by lowering the H/W ratio. However, for lateral pressure and material strength, we must comprehensively consider their impacts on the macro-strength and failure modes. The stabilization measures typically involve the implementation of a composite support system formed by rock mass grouting reinforcement combined with shotcrete lining, integrated with a multi-dimensional support system consisting of fully bonded rock bolts and pre-stressed anchor cables, supplemented by coordinated borehole pressure relief and stress compensation technologies. The control principles involve optimizing cross-sectional dimensions, enhancing structural integrity, effectively utilizing favorable stress environments, and rationally exploiting the intrinsic mechanical properties of rock masses.

3.4. Discussion of the effect of lateral pressure on the macro-strength of rock columns

The study in the previous two sections shows that the conventional knowledge that the macro-strength of rock increases with the increase of lateral pressure is derived based on the insignificant shape effect. When the failure mode of the rock column is a material failure-induced structural instability, the change of macro-strength conforms to the conventional knowledge. However, when the failure mode is a structural instability-induced material failure, the macro-strength decreases with the increased lateral pressure, and the rock column is more prone to instability and failure. Moreover, for rock columns with the H/W ratio and material strength determined, the sum of lateral pressure and macro-strength ($p + q$) is approximately equal (Fig. 10). The reason for this law will be explained below from two aspects.

On the one hand, a single element (RVE) is taken from the left and right sides of the rock column to analyze the stress state (Fig. 12a). As it is known, the tensile strength of rock as a brittle material is much lower than the compressive strength. When the rock column bends to the left side, the x- and y-directional stresses at the cross-section (Fig. 12b) show that the left element is in compression laterally and vertically. The lateral pressure is increased to a certain extent, the less likely the element is to be damaged. The right element is in the stress state of lateral compression and vertical tension, and an increase in lateral pressure will make the element more easily damaged. In addition, the neutral layer of the rock column moves to the compression side (concave side) with the increase of lateral pressure, which will make the tensile area larger and the element on the outermost side (convex side) of the rock column is more likely to be damaged first. Therefore, when the lateral pressure increases, the critical stress decreases for the rock column where the failure mode is the structural instability-induced material failure; that is, the disturbance resistance decreases, and the instability risk increases. For rock columns with the failure mode of material failure-induced structural instability, the H/W ratio typically remains relatively low. Consequently, bending effects can be effectively neglected under such geometric constraints. When subjected to lateral pressure, elements predominantly exist in a biaxial compressive stress state. During the elastic phase, enhanced lateral pressure generally improves the load-bearing capacity of individual elements through stress redistribution and confinement effects. This mesoscopic strengthening mechanism accordingly translates to increased macroscopic strength with progressive lateral pressure.

On the other hand, one can refer to the relevant elastic solid theory. Kerr and Tang [43] proposed a compressive stress formula for the buckling of a solid in the presence of lateral pressure for a slender rectangular elastic solid fixed at one end:

$$(p+q)_{cr} = \frac{\mu(\lambda+\mu)}{3(\lambda+2\mu)}\frac{\pi^2 W^2}{H^2} \tag{17}$$

where p is the lateral pressure, q is the critical compressive stress, taken as the macro-strength in this study, λ and μ is the Lamé constant. W and H are the width and height of the rectangular elastic solid, respectively.

From Eq. (17), note that the sum of the lateral pressure and the critical stress when the solid buckles is a constant value related to the material constants and the solid sizes. This means that for rock columns with determined material parameters and size, the higher the lateral pressure, the lower the critical stress of buckling, i.e., the more prone to instability and failure. In addition, it is also found that the larger the $H/$

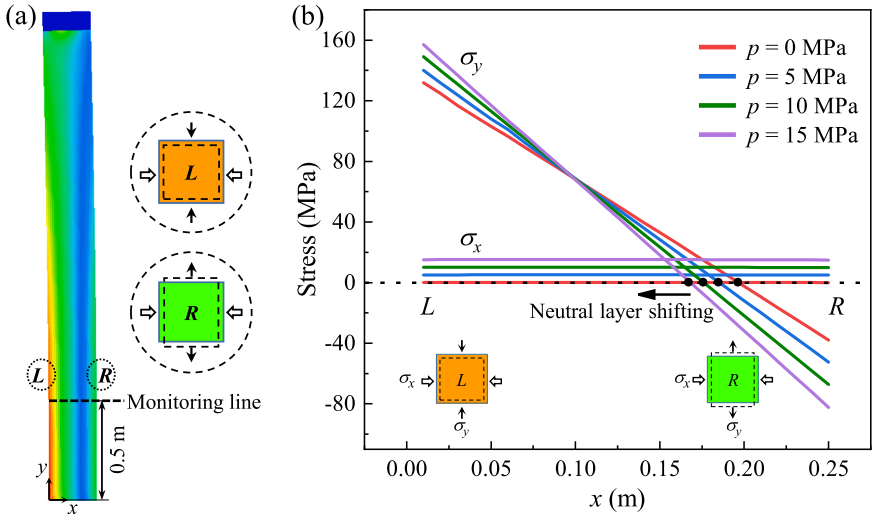

Fig. 12. Homogeneous model without considering material failure under lateral pressure: (a) Schematic diagram of the stress state of the elements on the left and right sides of the model, and (b) x- and y-direction stress distributions at the monitoring line of the model (0.5 m away from the bottom end), negative value indicates the tensile stress.

W ratio, the lower the critical stress of the model. Of particular interest is the fact that the strength of the material itself does not appear in the equation. This means that the critical stress of the model can only be increased by reducing the lateral pressure and *H/W* ratio or changing the material properties. That coincides with the traditional view of the mechanics of materials [39]. The primary reason that the sum of the lateral pressure and macro-strength ($p + q$) in Fig. 10 is approximately equal, rather than exactly equal, is that the heterogeneity of the material properties of the rock column and the failure of the elements are considered.

4. Conclusions

This study is devoted to an in-depth investigation of the key scientific issues of the mechanical response and the failure and instability mechanisms of slender rock columns with special geometrical effects under the synergy of external factor (lateral pressure) and internal factors (*H/W* ratio and material strength). Based on the elastic-brittle nature of the rock column material and the large deformation behavior of the structural body, a unified numerical scheme is adopted to incorporate the material failure and structural instability into a unified framework. A generalized model of rock columns at the engineering scale is established for the fundamental constituent unit rock columns of CJRM, and compression numerical tests under different combinations of lateral pressure, *H/W* ratio, and material strength are carried out. The rock columns' strength characteristics and failure modes were comprehensively analyzed from the material and structural perspectives.

The numerical results show that the effects of the three factors on the macro-strength and failure modes are significantly different. As an intrinsic factor of the rock column, the dominant effect of the *H/W* ratio is more potent than that of material strength. In contrast, the influence of the extrinsic factor, lateral pressure, is weaker and stage-specific. The location of the minimum value of macro-strength can determine the most unfavorable combination between the three factors. At a low *H/W* ratio and low material strength, the macro-strength and bending deformation of the rock column gradually increase with the increase of lateral pressure. The evolution process of the failure mode is as follows: material failure-induced structural instability → synergy and competition between material failure and structural instability → structural instability-induced material failure. The similarity in the effects of material strength and *H/W* ratio on rock columns lies in their ability to reduce the failure mode transition threshold as they increase. This accelerates the transition between failure modes, making the rock column more prone to large displacement and rotation. Ultimately, the failure mode is a structural instability-induced material failure. However, the two effects on the macro-strength are diametrically opposite; the increase in the material strength can improve the macro-strength, while the increase in the *H/W* ratio will reduce the macro-strength. When the failure mode of the rock column is the structural instability-induced material failure, the increase of lateral pressure will limit its bending deformation, inhibit crack development and expansion, and affect the stress (shear) distribution. Notably, in this case, an increase in lateral pressure can reduce macro-strength. These effects of lateral pressure heighten the instability risk, leading to more sudden and catastrophic failures. Compared to the conventional understanding of rock response to lateral pressure at low *H/W* ratios, which primarily focuses on material failure perspectives, this finding provides a broader perspective on the influence of lateral pressure under varying *H/W* ratios.

The transformation of failure modes is a dynamic evolutionary process of competition, synergy, and transformation between material failure and structural instability rather than an abrupt process. On the space composed of three factors and macro-strength, the failure mode demarcation line was established based on the variation trend of macro-strength and failure characteristics. According to the position of these demarcation lines, the failure modes of rock columns can be regulated by altering the three factors along macro-strength contours. Reducing the *H/W* ratio can mitigate structural instability, whereas changes in lateral pressure and material strength require a comprehensive evaluation of their combined effects on macro-strength and failure modes.

CRediT authorship contribution statement

Shiguo Feng: Writing – original draft, Visualization, Methodology, Investigation, Data curation, Conceptualization, Writing – review & editing. **Gen Li:** Supervision, Software, Methodology, Funding acquisition.

Declaration of Competing Interest

The authors declare that they have no known competing financial interests or personal relationships that could have appeared to influence the work reported in this paper.

Acknowledgements

This work is supported in part by the National Natural Science Foundation of China (42272330; 52079019), the Liaoning Province Science and Technology Plan Joint Program (Applied Basic Research Project) (2023JH2/101700340), and the Fundamental Research Funds for the Central Universities (DUT24ZD135).

References

[1] A. Spry, The origin of columnar jointing, particularly in basalt flows, J. Geol. Soc. Aust. 8 (1962) 191–216.
[2] L. Goehring, S.W. Morris, Scaling of columnar joints in basalt, J. Geophys. Res. 113 (2008) 196–199.
[3] A.C. Shi, M.F. Tang, Q.J. Zhou, Research of deformation characteristics of columnar jointed basalt at Baihetan hydropower station on Jinsha River, Chin. J. Rock. Mech. Eng. 10 (2008) 2079–2086.
[4] C.S. Zhang, J.R. Xu, H. Ji, N. Liu, S.H. Ni, Mechanical characteristics and relax control of columnar jointed basalt at Baihetan hydropower station, Chin. J. Rock. Mech. Eng. 41 (2022) 1297–1309.
[5] Q.X. Fan, X.T. Feng, W.L. Weng, Y.L. Fan, Q. Jiang, Unloading performances and stabilizing practices for columnar jointed basalt: A case study of Baihetan hydropower station, J. Rock. Mech. Geotech. Eng. 9 (2017) 1041–1053.
[6] Q. Jiang, X.T. Feng, Y.L. Fan, Q.X. Fan, G.F. Liu, S.F. Pei, S.Q. Duan, In situ experimental investigation of basalt spalling in a large underground powerhouse cavern, Tunn. Undergr. Space Technol. 68 (2017) 82–94.
[7] X.C. Que, Z.D. Zhu, Y.X. He, Z.H. Niu, H.N. Huang, Strength and deformation characteristics of irregular columnar jointed rock mass: A combined experimental and theoretical study, J. Rock. Mech. Geotech. Eng. 15 (2023) 429–441.
[8] X.C. Que, S. Zhu, Z.D. Zhu, J. Zhang, X.H. Xie, Z.H. Niu, Anisotropic characteristic strength and energy evolution of irregular columnar jointed rock masses before and after excavation, Rock. Mech. Rock. Eng. (2024).
[9] C.Y. Jin, S.G. Li, J.P. Liu, Anisotropic mechanical behaviors of columnar jointed basalt under compression, Bull. Eng. Geol. Environ. 77 (2018) 317–330.
[10] T. Zhang, W.Y. Xu, H.L. Wang, R.B. Wang, A.C. Shi, Experimental investigations on short-term and creep anisotropic mechanical behavior of artificial columnar jointed rock masses, Rock. Mech. Rock. Eng. 55 (2022) 5393–5413.
[11] Y.J. Xia, C.Q. Zhang, H. Zhou, J. Hou, G.S. Su, Y. Gao, N. Liu, H.K. Singh, Mechanical behavior of structurally reconstructed irregular columnar jointed rock mass using 3D printing, Eng. Geol. 268 (2020) 105509.
[12] D.C. Zhao, Y.J. Xia, C.Q. Zhang, N. Liu, C.A. Tang, H.K. Singh, J. Chen, P. Wang, A new method to investigate the size effect and anisotropy of mechanical properties of columnar jointed rock mass, Rock. Mech. Rock. Eng. 56 (2023) 2829–2859.
[13] Q.X. Meng, H.L. Wang, W.Y. Xu, Y.L. Chen, Numerical homogenization study on the effects of columnar jointed structure on the mechanical properties of rock mass, Int. J. Rock. Mech. Min. Sci. 124 (2019) 104127.
[14] Y.Y. Wang, B. Gong, C.A. Tang, Numerical investigation on anisotropy and shape effect of mechanical properties of columnar jointed basalts containing transverse joints, Rock. Mech. Rock. Eng. 55 (2022) 7191–7222.
[15] Y.H. Hatzor, X.T. Feng, S.J. Li, G. Yagoda-Biran, Q. Jiang, L.X. Hu, Tunnel reinforcement in columnar jointed basalts: The role of rock mass anisotropy, Tunn. Undergr. Space Technol. 46 (2015) 1–11.
[16] Z.J. Liu, H.B. Wang, C.Q. Zhang, B. Zhou, H. Zhou, Size dependences of the mechanical behaviors of basalt rock blocks with hidden joints analyzed using a hybrid DFN-FDEM model, Eng. Fract. Mech. 258 (2021) 108078.
[17] K. Du, X.F. Li, R. Su, M. Tao, S.Z. Lv, J. Luo, J. Zhou, Shape ratio effects on the mechanical characteristics of rectangular prism rocks and isolated pillars under uniaxial compression, Int. J. Min. Sci. Technol. 32 (2022) 347–362.

[18] Y.Z. Zhao, L.Q. Huang, X.B. Li, C.J. Li, Z.H. Chen, Z.W. Cao, Failure modes and slabbing mechanisms of hard rock with different height-to-width ratios under uniaxial compression, Trans. Nonferrous Met. Soc. China 32 (2022) 3699–3713.
[19] D.Y. Li, C.C. Li, X.B. Li, Influence of sample height-to-width ratios on failure mode for rectangular prism samples of hard rock loaded in uniaxial compression, Rock. Mech. Rock. Eng. 44 (2011) 253–267.
[20] M. Wang, W. Wan, Y.L. Zhao, Experimental study on crack propagation and coalescence of rock-like materials with two pre-existing fissures under biaxial compression, Bull. Eng. Geol. Environ. 79 (2020) 3121–3144.
[21] K. Mogi, London. Experimental rock mechanics, CRC Press, 2006.
[22] J. Deng, D.S. Gu, Buckling mechanism of pillar rockbursts in underground hard rock mining, Geomech. Geoengin. 13 (2018) 168–183.
[23] S.E. Rosales Garzon, Analytical solution for assessing continuum buckling in sedimentary rock slopes based on the tangent-modulus theory, Int. J. Rock. Mech. Min. Sci. 90 (2016) 53–61.
[24] Q.S. Wang, R.T. Zhang, H. Zheng, P.Z. Zhou, An analytical solution of critical sliding displacement for the flexural buckling failure of layered rock slopes, Int. J. Rock. Mech. Min. Sci. 169 (2023) 105450.
[25] Z.D. Zhu, T.H. Qin, S.H. Wang, L.G. Wang, L.Z. Sun, Study of anisotropic constitutive model of columnar jointed rock masses based on Cosserat theory, Chin. J. Rock. Mech. Eng. 29 (2010) 4068–4076.
[26] G. Li, X.F. Cheng, L.H. Hu, C.A. Tang, The material-structure duality of rock mass: Insight from numerical modeling, Int. J. Rock. Mech. Min. Sci. 144 (2021) 104821.
[27] G. Li, X.F. Cheng, L.H. Hu, Z.G. Tao, C.A. Tang, Rock failure and instability from a structural perspective: Insights from the shape effect, Rock. Mech. Rock. Eng. 55 (2022) 937–952.
[28] S.G. Feng, G. Li, L. Zheng, The material-structure duality in rock mass failure and instability: Concept, unified numerical scheme, and benchmark, Comput. Geotech. 173 (2024) 106589.
[29] Q. Jiang, B. Wang, X.T. Feng, Q.X. Fan, Z.L. Wang, S.F. Pei, S. Jiang, In situ failure investigation and time-dependent damage test for columnar jointed basalt at the Baihetan left dam foundation, Bull. Eng. Geol. Environ. 78 (2019) 3875–3890.
[30] X.C. Que, Z.D. Zhu, Z.H. Niu, H.N. Huang, Deformation and strength anisotropy of columnar jointed rock mass with different cross-sectional shapes, Rock. Soil Mech. 42 (2021) 2416–2426.
[31] X.C. Que, Z.D. Zhu, L.M. Zhou, Z.H. Niu, H.N. Huang, Strength and failure characteristics of an irregular columnar jointed rock mass under polyaxial stress conditions, Rock. Mech. Rock. Eng. 55 (2022) 7223–7242.
[32] C.A. Tang, Numerical simulation of progressive rock failure and associated seismicity, Int. J. Rock. Mech. Min. Sci. 34 (1997) 249–261.
[33] G. Li, C.A. Tang, A statistical meso-damage mechanical method for modeling trans-scale progressive failure process of rock, Int. J. Rock. Mech. Min. Sci. 74 (2015) 133–150.
[34] W. Weibull, A statistical distribution function of wide applicability, J. Appl. Mech. 18 (1951) 293–297.
[35] J.W. Ju, Isotropic and anisotropic damage variables in continuum damage mechanics, J. Eng. Mech. 116 (1990) 2764–2770.
[36] J. Lemaitre, Coupled elasto-plasticity and damage constitutive equations, Comput. Meth. Appl. Mech. Eng. 51 (1985) 31–49.
[37] O.C. Zienkiewicz, R.L. Taylor, D. Fox, The Finite Element Method for Solid and Structural Mechanics, Butterworth-Heinemann, Oxford, 2014.
[38] P. Lin, J. Shi, P.C. Wei, Q.X. Fan, Z.L. Wang, Shallow unloading deformation analysis on Baihetan super-high arch dam foundation, Bull. Eng. Geol. Environ. 78 (2019) 5551–5568.
[39] J.M. Gere, B.J. Goodno, Mechanics of materials, Cengage learning, Canada, 2012.
[40] T. Zhang, W.Y. Xu, J.R. Xu, Experimental and numerical investigations on the mechanical behavior of basalt in the dam foundation of the Baihetan hydropower station, Int. J. Geomech. 22 (2022) 04021272.
[41] G.Z. Sun, Y. Sun, Principle of rock mass mechanics, Science Press, Beijing, 2011.
[42] S.L. Qiu, X.T. Feng, C.Q. Zhang, T.B. Xiang, Estimation of rockburst wall-rock velocity invoked by slab flexure sources in deep tunnels, Can. Geotech. J. 51 (2014) 520–539.
[43] A.D. Kerr, S. Tang, The instability of a rectangular elastic solid, Acta Mech. 4 (1967) 43–63.

Shiguo Feng is a Ph.D. candidate at the School of Infrastructure Engineering, Dalian University of Technology. His research focuses on the fracture and instability mechanisms of rock masses under multi-field coupling effects, as well as related numerical methods and simulations.